Postprint of: Koziel S., Pietrenko-Dabrowska A., Design-oriented computationally-efficient feature-based surrogate modelling of multi-band antennas with nested kriging, AEU - International Journal of Electronics and Communications, Vol. 120 (2020), 153202, DOI: 10.1016/j.aeue.2020.153202

Design-Oriented Computationally-Efficient Feature-Based Surrogate Modelling of Multi-Band Antennas with Nested Kriging

Slawomir Koziel[1,2] and Anna Pietrenko-Dabrowska[*2]

[1] Engineering Optimization & Modelling Center, Reykjavik University, 101 Reykjavik, Iceland, koziel@ru.is,
[2] Faculty of Electronics, Telecommunications and Informatics, Gdansk University of Technology, 80-233 Gdansk, Poland, anna.dabrowska@pg.edu.pl

Corresponding author: anna.dabrowska@pg.edu.pl

Keywords: Antenna design; surrogate modelling; approximation models; simulation-driven design; kriging interpolation; response features.

Abstract

Design of modern antenna structures heavily depends on electromagnetic (EM) simulation tools. EM analysis provides reliable evaluation of increasingly complex designs but tends to be CPU intensive. When multiple simulations are needed (e.g., for parameters tuning), the aggregated simulation cost may become a serious bottleneck. As one possible way of mitigating the issue, the recent literature fosters utilization of faster representations, or surrogates, of the system at hand. Notwithstanding, conventional models are severely affected by the curse of dimensionality. In practice, modelling of antenna structures described by no more than a few parameters over narrow parameter ranges is possible. In the context of the structural complexity of modern antennas, this is hardly acceptable. This paper presents a novel technique for cost-efficient design-oriented modelling of multi-band antennas. Our approach integrates a recently reported nested kriging framework and the response feature technology. This combination enables rendering of reliable surrogates valid within broad ranges of geometry parameters while using small training data sets. Benchmarking against conventional modelling methods demonstrates superiority of the proposed framework in terms of both the predictive power of the surrogate and its setup cost. Design applications for antenna optimization are discussed as well.

1. Introduction

Recent years observed a steady increase of performance requirements imposed on antenna systems. These requirements are partially related to the emergence of new application areas, such as internet of things [1], [2], wearable devices [3], or tele-medicine appliances [4] but also growing demands for additional functionalities, e.g., multi-functionality [5], multi-band operation [6], [7], circular polarization [8], [9], MIMO operation [10], [11], polarization/pattern diversity [12], or band notches in the case of ultra-wideband antennas [13]. Design of antennas meeting stringent specifications is a difficult endeavour, further aggravated by various constraints, related to physical size of the structure (miniaturization [14], [15]). Consequently, antenna geometries are becoming increasingly complex and described by more and more parameters. Due to the same complexity, EM-simulation tools are nowadays indispensable both for reliable characterization and for carrying out the design process. Unfortunately, common EM-driven tasks such as parametric optimization [16,17], yield estimation [18], or tolerance-aware design [19,20], typically involve massive simulations the computational cost of which may be of practical concern if not unmanageable.

Utilization of faster representations (or surrogates) of full-wave simulation models is frequently recommended to alleviate the high CPU cost issue [21], [22]. The surrogates can be classified into two groups: physics-based (exploiting the system-specific knowledge, normally in the form of lower-fidelity models) and approximation (or data-driven) ones [21]. One of the most recognized physics-based surrogate-assisted techniques in high-frequency electronics is space mapping (SM) [23], [24]. Other examples, more relevant to antenna design, include response correction algorithms [25],

feature-based optimization [26], or adaptive response scaling [27]. Yet, in the case of antennas, construction of reliable physics-based surrogates requires the employment of coarse-discretization EM simulations as the underlying low-fidelity models. These are relatively expensive in terms of the computational cost [28], which may limit the efficacy of the surrogate-based procedures.

A potentially attractive alternative to physics-based models are data-driven surrogates, constructed by approximating sampled simulation data. Their popularity follows from some important advantages: no need for physical insight into the system of interest, transferability between application areas, low evaluation cost, and widespread access (e.g., DACE [29], SUMO [30], UQlab [31]). Commonly used data-driven modelling techniques include kriging [32],[33], radial basis functions (RBF) [34], Gaussian process regression (GPR) [35], neural networks [36],[37], support vector regression [38],[39], polynomial response surfaces [40], or fuzzy models [41]. Unfortunately, approximation surrogates are largely affected by the curse of dimensionality, i.e., a rapid growth of the number of training samples as a function of the system parameters and their ranges [42]. In particular, data-driven modelling of multi-band antennas is seriously hindered beyond a few parameters of rather limited ranges. The latter is by no means sufficient in the design of antenna structures featuring complex topologies. The shortcomings of conventional approximation models stimulated the development of improved methods, e.g., high-dimensional model representation (HDMR) [43], feature-based modelling [44], or orthogonal matching pursuit (OMP) [45]. These address certain aspects of the modelling process and are applicable within particular scenarios, e.g., weak variable interaction (HDMR), or clearly dominating subsets of basis

functions (OMP). Other techniques work around computational complexity of training data acquisition by merging simulation data of various fidelities. The examples include space mapping [46],[47], Bayesian model fusion [48], co-kriging [49], or two-stage GPR [50]. Yet another option is domain confinement, where the surrogate is constructed within a parameter space region that contains high-quality designs (from the point of view of the relevant figures of interest) [51]-[54]. Approximation of such a subset is normally obtained from a set of pre-optimized reference designs with detailed formulation of the domain varying between implementations, e.g., [51]-[54]. Notwithstanding, domain confinement permits construction of reliable surrogates within wide ranges of parameters and operating conditions even in spaces of relatively high dimensionality. The technique of [54] has been further developed in [55] and [56] by enhancing the design of experiments procedure, leading to the improved predictive power of the surrogate without increasing the training data acquisition costs.

In this paper, a novel modelling technique is proposed which incorporates a response feature methodology [44] into the nested kriging framework [54]. The primary purpose of the latter is to confine the surrogate model domain. The actual surrogate is constructed as the level of selected feature points of the antenna responses, which "flattens" the functional landscape to be approximated. Ultimately, a combination of both methodologies allows for setting up antenna models within broad parameter ranges using significantly reduced training data sets, both w.r.t. conventional models and the nested kriging operating on the entire responses. Here, frequency/level coordinates of the resonances as well as bandwidth-defining –10 dB levels of the reflection characteristic are employed as the response features. The benchmark set comprises a dual- and triple-

band antenna. Our approach is favourably compared to the conventional data-driven models (kriging and RBF), as well as the nested kriging model, both in terms of the surrogate predictive power and the computational cost of training data acquisition.

2. Nested Kriging Modelling with Response Features

This section briefly recalls the nested kriging modelling technique (see [54] for more details), as well as provides an outline of the response feature methodology [44]. Subsequently, it formulates the proposed modelling framework, accommodating both aforementioned methods.

2.1. Nested Kriging Modelling

In the nested kriging technique [54], a confined surrogate model domain is determined based on a set of reference designs $\boldsymbol{x}^{(j)} = [x_1^{(j)} \ldots x_n^{(j)}]^T$, $j = 1, \ldots, p$, pre-optimized w.r.t. the selected performance vectors $\boldsymbol{f}^{(j)} = [f_1^{(j)} \ldots f_N^{(j)}]$. Here, f_k, $k = 1, \ldots, N$, are the performance figures of interest (e.g., target antenna operating frequencies in the case of multi-band antennas as considered in this paper). The objective space F is defined by the user-defined ranges for f_k, $f_{k.\min} \le f_k^{(j)} \le f_{k.\max}$, $k = 1, \ldots, N$, that should be covered by the surrogate. It is advisable for $\{\boldsymbol{f}^{(j)}\}$ to be distributed within F in a uniform manner [54].

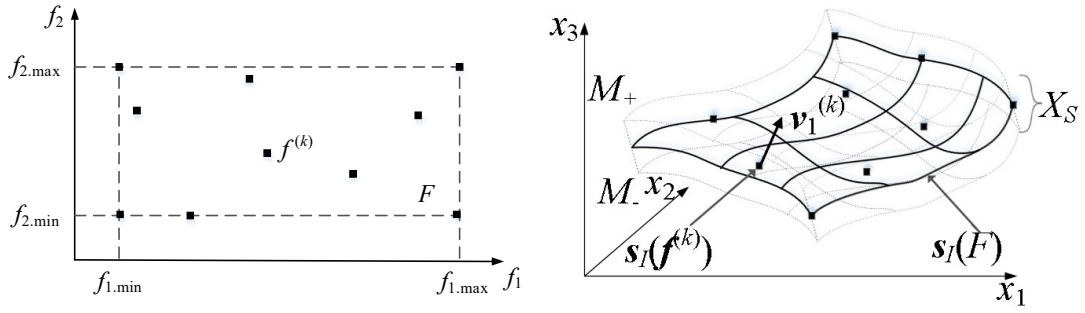

(a) (b)

Fig. 1. The concept of nested kriging modelling illustrated for $N = 2$ and $n = 3$: (a) reference designs and the objective space F; (b) the image $s_I(F)$ of F and the normal vector $v_1^{(k)}$ at $f^{(k)}$, the manifolds M_- and M_+, along with the surrogate model domain X_S (defined as the orthogonal extension of $s_I(F)$).

The nested kriging technique utilizes two levels of models: the first one to establish the confined domain, and the second-level model being the actual surrogate. Both models are implemented using kriging interpolation [57]. The first-level model $\boldsymbol{s}_I(\boldsymbol{f})$ maps the objective space F into the design space X, with $\{\boldsymbol{f}^{(j)},\boldsymbol{x}^{(j)}\}$ being the training points (cf. Fig. 1). The image $\boldsymbol{s}_I(F) \subset X$ of F delivers the first approximation of the region in which the surrogate is to be established. Because the first-level model is identified using limited information (in practice, only a small number of reference designs is available), it does not give a complete account for the location of the optimum designs corresponding to all $\boldsymbol{f} \in F$. In order to ensure that the domain contains these, $\boldsymbol{s}_I(F)$ has to be expanded. This is achieved through its orthogonal extension. Let us define the following quantities: an orthonormal basis $\{\boldsymbol{v}_n^{(k)}(\boldsymbol{f})\}$, $k = 1, \ldots, n - N$, of vectors normal to $\boldsymbol{s}_I(F)$ at $\boldsymbol{f}$, and the parameter variations $\boldsymbol{x}_d = \boldsymbol{x}_{\max} - \boldsymbol{x}_{\min}$ within $\boldsymbol{s}_I(F)$, where $\boldsymbol{x}_{\max} = \max\{\boldsymbol{x}^{(k)}, k = 1, \ldots, p\}$ and $\boldsymbol{x}_{\min} = \min\{\boldsymbol{x}^{(k)}, k = 1, \ldots, p\}$. In addition, the vector of the coefficients of the extension is defined a

$$\boldsymbol{\alpha}(\boldsymbol{f}) = [\alpha_1(\boldsymbol{f}) \ldots \alpha_{n-N}(\boldsymbol{f})]^T = \frac{D}{2}\left[|\, \boldsymbol{x}_d \boldsymbol{v}_n^{(1)}(\boldsymbol{f})\,| \;\ldots\; |\, \boldsymbol{x}_d \boldsymbol{v}_n^{(n-N)}(\boldsymbol{f})\,|\right]^T \tag{1}$$

where D is a user-defined thickness parameter which sets the "span" of the extension (i.e., the ratio of the lateral to the tangential size of the surrogate model domain). The confined domain X_S is located between the manifolds M_+ and M_- determined using the coefficients α_k as (see Fig. 1(b))

$$M_{\pm} = \left\{\boldsymbol{x} \in X : \boldsymbol{x} = \boldsymbol{s}_I(\boldsymbol{f}) \pm \sum_{k=1}^{n-N} \alpha_k(\boldsymbol{f}) \boldsymbol{v}_n^{(k)}(\boldsymbol{f})\right\} \tag{2}$$

The second-level model, being the actual surrogate, is constructed within the domain X_S. The training set comprises pairs $\{\boldsymbol{x}_B^{(k)}, \boldsymbol{R}(\boldsymbol{x}_B^{(k)})\}_{k = 1, \ldots, NB}$, with $\boldsymbol{R}$ being the EM-simulation model of the antenna at hand.

The important advantage of the above formulation is that it facilitates uniform sampling, as well as surrogate model optimization through an auxiliary mapping from the n-dimensional unit interval $[0,1]^n$ onto X_S. The mapping is a composition of the following transformations: h_1 from $[0,1]^n$ onto a Cartesian product $F \times [-1,1]^{n-N}$ defined as

$$\begin{aligned}\boldsymbol{y} = h_1(\boldsymbol{z}) = h_1([z_1 \ldots z_n]^T) = [f_{1.\min} + z_1(f_{1.\max} - f_{1.\min}) \ \ldots \\ \ldots f_{N.\min} + z_N(f_{N.\max} - f_{N.\min})] \times [-1 + 2z_{N+1} \ \ldots \ -1 + 2z_n]\end{aligned} \tag{3}$$

where $\boldsymbol{z} = [z_1 \ \ldots \ z_n]^T \in [0,1]^n$, and h_2 from $F \times [-1,1]^{n-N}$ onto X_S, defined as

$$\begin{aligned}\boldsymbol{x} = h_2(\boldsymbol{y}) = h_2([y_1 \ldots y_n]^T) = \boldsymbol{s}_I([y_1 \ \ldots \ y_N]^T) + \\ + \sum_{k=1}^{n-N} y_{N+k} \alpha_k([y_1 \ \ldots \ y_N]^T) \boldsymbol{v}_n^{(k)}([y_1 \ \ldots \ y_N]^T)\end{aligned} \tag{4}$$

The overall transformation H from $[0,1]^n$ onto X_S is then a composition of h_1 and h_2

$$\boldsymbol{x} = H(\boldsymbol{z}) = h_2(h_1(\boldsymbol{z})) \tag{5}$$

As mentioned before, the mapping H facilitates uniform sampling in X_S as a set of uniformly distributed samples $\{\boldsymbol{x}_B^{(k)}\}$ in X_S can be obtained as $\{H(\boldsymbol{z}_B^{(k)})\}$, where $\{\boldsymbol{z}_B^{(k)}\}$ is the uniform data set in $[0,1]^n$. Furthermore, it is possible to optimize the surrogate model in X_S by operating within the unit hypercube and then employing the mapping H (cf. Section 2.4). Finally, a good initial point for parametric optimization within X_S can be conveniently generated using the first-level model as $\boldsymbol{x}_0 = \boldsymbol{s}_I(\boldsymbol{f}_t)$.

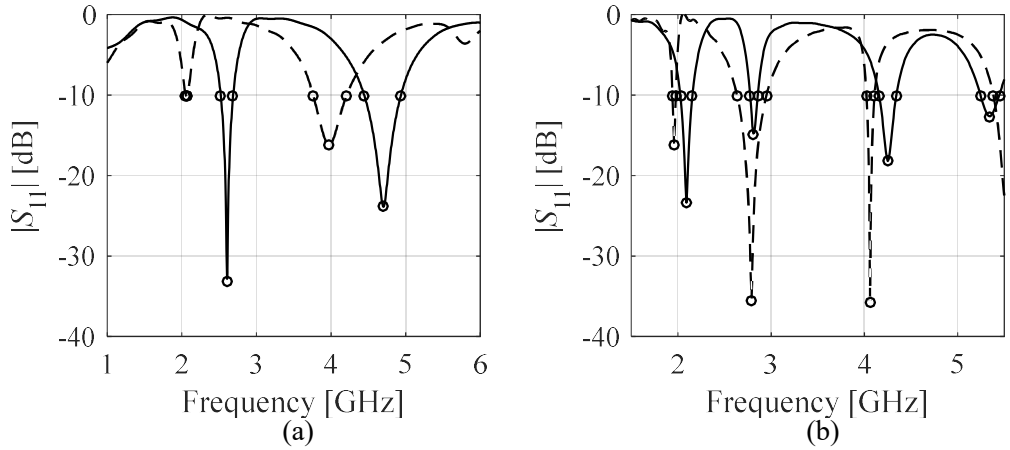

Fig. 2. Example input characteristics and the feature points (here, corresponding to antenna resonances and –10 dB reflection levels): (a) dual-band antenna, (b) triple-band antenna.

2.2. Response Features

The response feature approach [26], [58], reformulates the design problem in terms of the characteristic points (features) of the system response. The points are selected so as to be sufficient to evaluate the design quality. The underlying rationale is that the dependence of the feature point coordinates on design variables is normally only weakly nonlinear in comparison to the nonlinearity of the entire responses. In many cases, especially multi-band antennas [58], this can make a significant difference in terms of the computational cost of both modelling process and design optimization.

In the design of multi-band antennas, the frequency locations of the antenna resonances and the points corresponding to –10 dB level of reflection are of interest. These points can be extracted from the EM simulation results and then employed to allocate the resonances at the required operating frequencies and/or optimize the antenna for maximum bandwidth (see Fig. 2).

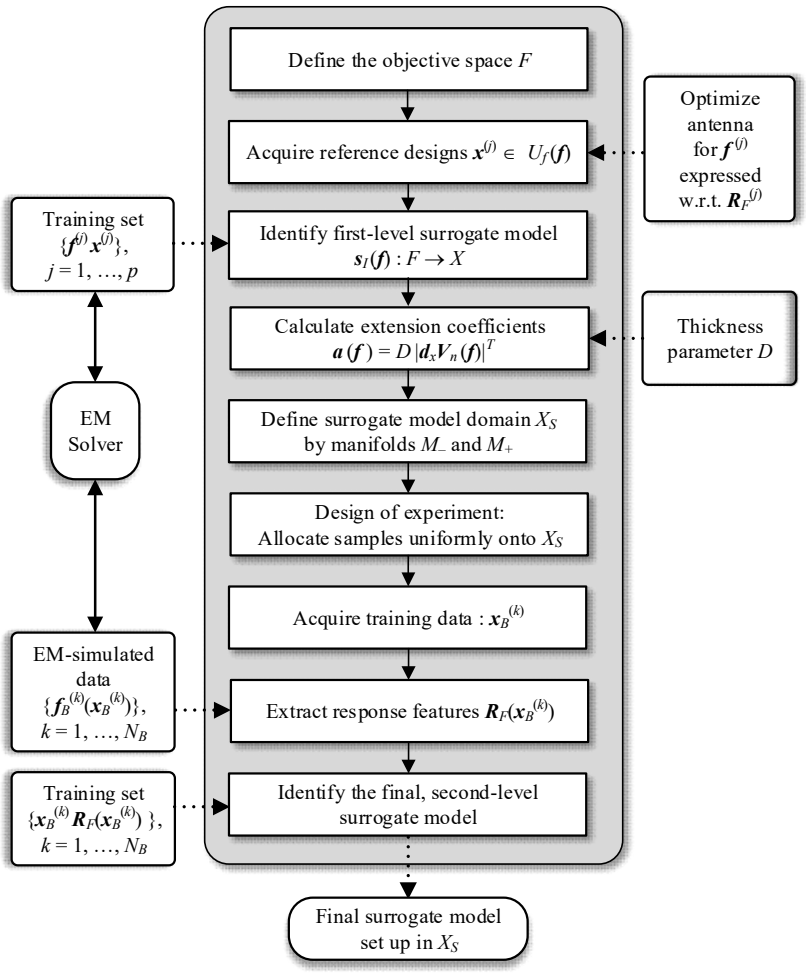

Fig. 3. Flow diagram of the feature-based nested kriging modelling methodology.

2.3. Incorporation of Response Features into Nested Modelling Framework

Let us denote the feature points referring to p antenna resonances as $\boldsymbol{R}_F(\boldsymbol{x}) = [f_1(\boldsymbol{x})\ f_2(\boldsymbol{x})\ \ldots\ f_p(\boldsymbol{x})\ \ l_1(\boldsymbol{x})\ \ l_2(\boldsymbol{x})\ \ldots\ l_p(\boldsymbol{x})]^T$, where f_k and l_k stand for their frequency and level coordinates, $k = 1, \ldots, p$, respectively. In feature-based nested kriging, both the first-level surrogate and the domain definition are identical to that presented in Section 2.4. Whereas the training set for the second-level surrogate consists of the pairs of the response feature vectors $\boldsymbol{R}_F(\boldsymbol{x}_B^{(k)})$ (rather than the original responses) and the corresponding training designs $\{\boldsymbol{x}_B^{(k)}, \boldsymbol{R}_F(\boldsymbol{x}_B^{(k)})\}_{k = 1, \ldots, NB}$. Assuming that the design objectives can be uniquely

quantified using the selected feature points (the surrogate merely provides a prediction about the feature coordinates at the design of interest $\boldsymbol{x} \in X_S$) modelling of $\boldsymbol{R}_F$ rather than $\boldsymbol{R}$ does not lead to any loss of information from design purposes point of view.

The steps undertaken to construct the surrogate model within the feature-based nested kriging framework are the following (see also Fig. 3). First, the objective space F is defined, e.g., by the ranges of the antenna operating frequencies to be covered by the model (cf. Section 2.1). Subsequently, the reference designs $\boldsymbol{x}^{(j)}$, $j = 1, \ldots, p$, are obtained and utilized for setting up the first-level surrogate $\boldsymbol{s}_1$.

Next, the surrogate model domain is established (cf. (3)) with the use of the normal vectors $\boldsymbol{v}_n^{(k)}$, $k = 1, \ldots, n - N$, and the expansion coefficients α_k. Within that domain, the training data $\{\boldsymbol{x}_B^{(k)}\}_{k = 1, \ldots, NB}$, is allocated by transforming the normalized training data samples $\{\boldsymbol{z}_B^{(k)}\}_{k = 1, \ldots, NB}$, from the unit hypercube $[0,1]^n$ through the mapping H (6). Here, the normalized samples are obtained using Latin Hypercube Sampling [59]. Subsequently, the EM model data $\boldsymbol{R}(\boldsymbol{x}_B^{(k)})$, $k = 1, \ldots, N_B$, is acquired and the response features $\boldsymbol{R}_F(\boldsymbol{x}_B^{(k)})$, $k = 1, \ldots, N_B$, are extracted. Finally, the surrogate is identified based on the training set $\{\boldsymbol{x}_B^{(k)}, \boldsymbol{R}_F(\boldsymbol{x}_B^{(k)})\}_{k = 1, \ldots, NB}$. The surrogate model yields the feature point coordinates of the antenna response corresponding to any design $\boldsymbol{x}$ from the constrained domain X_S.

3. Results

This section provides a numerical verification of the modelling framework of Section 2, as well as comparisons with benchmark procedures: the conventional approximation models (kriging and RBF) and the nested kriging model [54]. Table 1 reports the modelling errors (average relative RMS), estimated based on 100 independent

random test points. It should be noted that in the case of the feature-based nested kriging, the errors of the frequency coordinates of the characteristic points are presented.

The proposed methodology has been demonstrated using multiband antennas: a dual- (Antenna I) and triple-band antenna (Antenna II), shown in Fig. 4(a) and Fig. 6(a), respectively. Both antennas are implemented on the RO4350 substrate ($\varepsilon_r = 3.48$, $h = 0.762$ mm) and fed by a coplanar waveguide.

Antenna I [60] is described by the following design variables: $\boldsymbol{x} = [l_1\ l_2\ l_3\ w_1\ w_2\ w_3]^T$, with $l_0 = 30$, $w_0 = 3$, $s_0 = 0.15$ and $o = 5$ being fixed (all dimensions in mm). The geometry parameters of Antenna II [61] are: $\boldsymbol{x} = [l_1\ l_2\ l_3\ l_4\ l_5\ w_1\ w_2\ w_3\ w_4\ w_5]^T$; where $l_0 = 30$, $w_0 = 3$, $s_0 = 0.15$ and $o = 5$ are fixed (all dimensions in mm). Antenna. The computational models of both structures are implemented in CST Microwave Studio and simulated using its time-domain solver.

The surrogate models have been constructed using the following sizes of training data sets: 20, 50, 100, 200, 400, and 800 samples (the adopted value of the thickness parameter was $D = 0.05$).

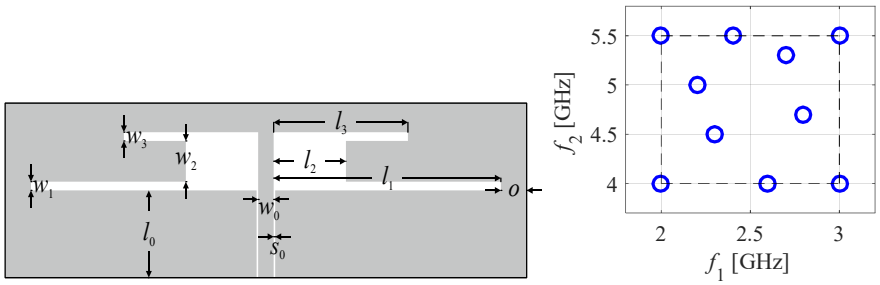

(a) (b)

Fig. 4. Uniplanar dual-band dipole antenna [60]: (a) geometry, (b) allocation of the reference designs in the objective space.

3.1. Dual-Band Antenna

The goal is to construct the surrogate model valid for the following ranges of operating frequencies: 2.0 GHz $\leq f_1 \leq$ 3.0 GHz (lower band), and 4.0 GHz $\leq f_2 \leq$ 5.5 GHz (upper band). The reference designs $\boldsymbol{x}^{(j)}$, j = 1, …, 10, are allocated as shown in Fig. 4(b). The lower and upper bounds for design variables, derived from $\boldsymbol{x}^{(j)}$, are $\boldsymbol{l}$ = [27 5.0 16.5 0.22 1.8 0.5]^T, and $\boldsymbol{u}$ = [40 12 23.5 0.6 4.3 2.7]^T.

The results presented in Table 1 reveal that the feature-based surrogate is far more accurate than the other benchmark models. A remark should be made that the model predictive power fluctuates for training data set sizes comprising more than 100 samples. This is due to the fact that the variance of the model error estimation and the error itself, here, around a fraction of percent, are at a similar level.

In the following, the examples of design applications of the feature-based nested kriging model for antenna optimization are presented. Table 2 and Fig. 5 show the results obtained for the surrogate set up with 50 training samples and four selected pairs of the target operating frequencies. It should be emphasized that the predictions yielded by the surrogate are indeed very accurate. As a matter of fact, even the initial designs obtained for the target vector $\boldsymbol{f}_t$ with the first level model as $\boldsymbol{x}^{(0)} = \boldsymbol{s}_1(\boldsymbol{f}_t)$ are of high quality (see Fig. 5).

3.2. Triple-Band Antenna

In the case of Antenna II, we aim at constructing the surrogate valid for the operating frequencies f_k, k = 1, 2, 3, $f_2 = f_1k_1$, $f_3 = f_2k_2$, within the following ranges: 1.5 GHz $\leq f_1 \leq$ 2.5 GHz, 1.2 $\leq k_1 \leq$ 1.6, and 1.2 $\leq k_2 \leq$ 1.6. Here, the objective space consists of the vectors $[f_1\ k_1\ k_2]^T$, and the operating frequencies are recalculated as above. Figure 6(b) shows the allocation of the reference designs (detailed data can be found in [61]).

The lower and upper bounds for design variables are: $\boldsymbol{l}$ = [30 5.0 20 5.0 15 0.2 0.2 0.2 0.2 0.2]^T, and $\boldsymbol{u}$ = [50 15 30 15 21 2.2 4.2 2.2 4.2 2.2]^T. Table 3 reports the modelling errors (average relative RMS), calculated based on 100 independent random test points.

Table 1 Modelling Results for Antenna I

Number of Training Samples	Relative RMS Error			
	Conventional Kriging Model	Conventional RBF	Nested Kriging Model [54]	Feature-based Nested Kriging [this work]
20	24.5 %	26.3%	19.0 %	1.43%
50	21.7 %	24.9 %	9.9 %	0.51%
100	17.3 %	19.8 %	6.4 %	0.39%
200	12.6 %	14.3 %	4.4 %	0.56%
400	9.3 %	10.5 %	3.8 %	0.43%
800	7.2 %	8.7 %	3.4 %	0.46%

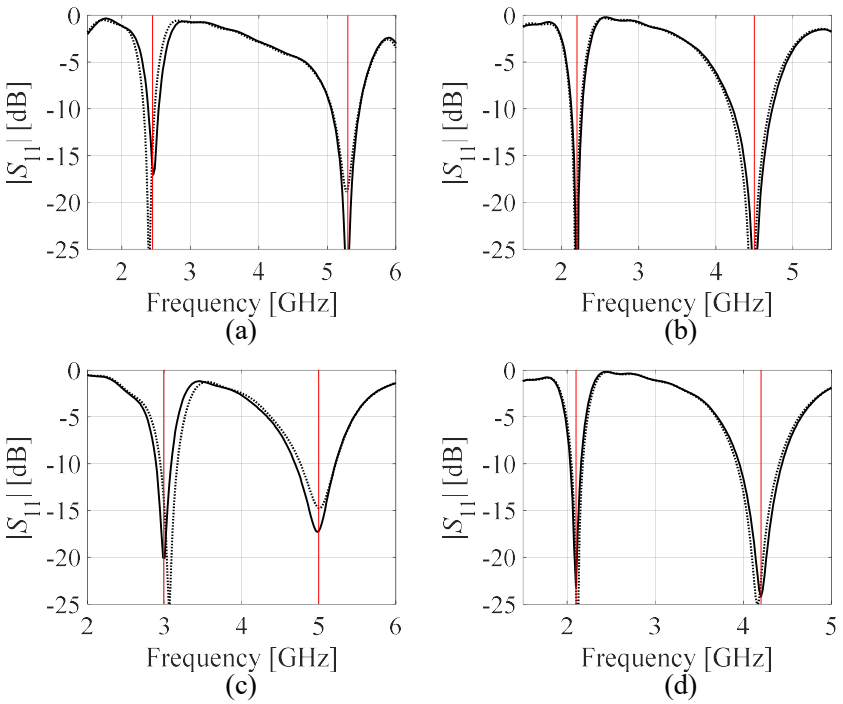

Fig. 5. Optimization results for Antenna I using feature-based nested kriging: EM-simulated antenna responses at the initial designs (…..) obtained with the surrogate, and the optimized responses (—). Required operating frequencies are marked using vertical lines: (a) f_1 = 2.45 GHz, f_2 = 5.3 GHz, (b) f_1 = 2.2 GHz, f_2 = 4.5 GHz, (c) f_1 = 3.0 GHz, f_2 = 5.0 GHz, and (d) f_1 = 2.1 GHz, f_2 = 4.2 GHz.

Table 2 Optimization Results for Antenna I

Target Operating Conditions		Geometry Parameter Values [mm]					
f_1 [GHz]	f_2 [GHz]	l_1	l_2	l_3	w_1	w_2	w_3
2.45	5.30	33.78	8.63	18.16	0.30	2.11	1.50
2.20	4.50	34.99	6.62	18.60	0.44	3.89	1.83
3.00	5.00	28.69	9.75	19.80	0.37	2.75	1.09
2.10	4.20	36.42	6.32	19.79	0.45	3.97	1.81

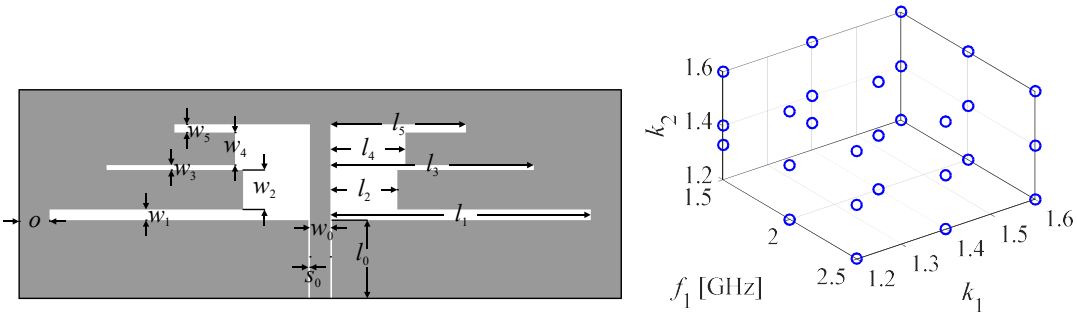

(a) (b)

Fig. 6. Uniplanar triple-band dipole antenna [52]: (a) geometry, (b) allocation of the reference designs in the objective space.

Table 3 Modelling Results for Antenna II

Number of Training Samples	Relative RMS Error			
	Conventional Kriging Model	Conventional RBF	Nested Kriging Model [54]	Feature-based Nested Kriging [this work]
20	28.5 %	30.1 %	38.9 %	2.65 %
50	22.7 %	23.5 %	16.0 %	0.25 %
100	19.9 %	19.8 %	11.2 %	0.22 %
200	18.6 %	19.2 %	9.9 %	0.19 %
400	17.2 %	18.8 %	9.7 %	0.14 %
800	16.8 %	17.4 %	7.8 %	0.20 %

Table 4 Optimization Results for Antenna II

Target Operating Frequencies [GHz]			Geometry Parameters [mm]									
f_1	f_2	f_3	l_1	l_2	l_3	l_4	l_5	w_1	w_2	w_3	w_4	w_5
1.6	2.56	4.09	39.97	5.40	32.19	8.56	21.82	0.22	0.70	0.37	1.42	0.83
1.8	2.34	3.51	39.98	7.12	33.85	7.00	23.45	0.74	1.49	0.21	1.82	0.75
2.1	2.94	4.12	37.61	10.36	31.03	10.73	22.85	051	1.43	1.17	1.26	0.41
2.4	3.36	5.04	36.20	12.06	28.39	11.83	21.34	0.59	1.15	1.15	0.75	0.39

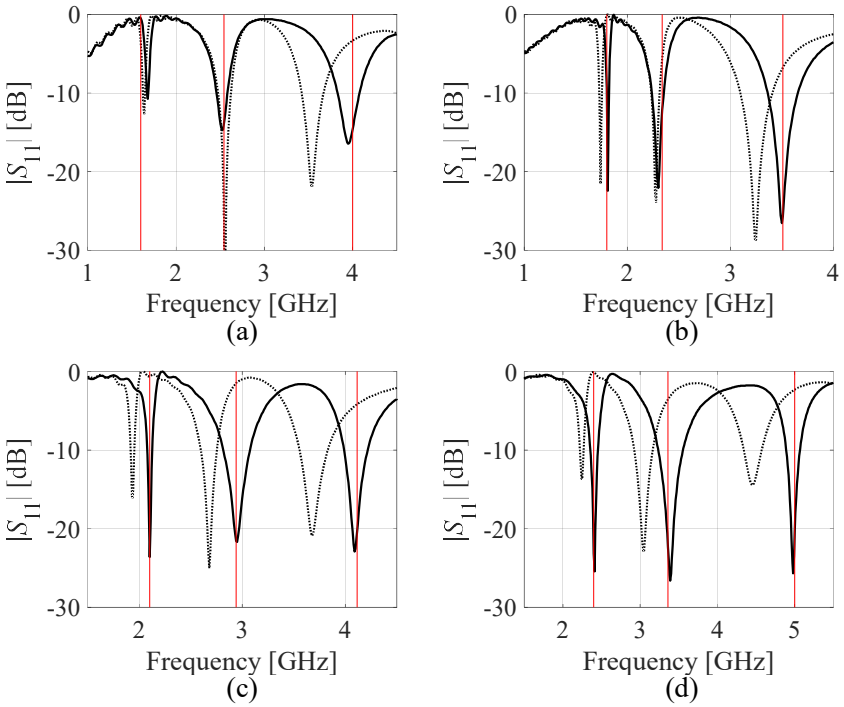

Fig. 7. Optimization results for Antenna II using feature-based nested kriging: EM-simulated antenna responses at the initial designs (…..) obtained with the surrogate, and the optimized responses (—). Required operating frequencies are marked using vertical lines: (a) f_1 = 1.6 GHz, k_1 = 1.6, k_2 = 1.6 (f_2 = 2.56 GHz, f_3 = 4.09 GHz), (b) f_1 = 1.8 GHz, k_1 = 1.3, k_2 = 1.5 (f_2 = 2.34 GHz, f_3 = 3.51 GHz), (c) f_1 = 2.1 GHz, k_1 = 1.4, k_2 = 1.4 (f_2 = 2.94 GHz, f_3 = 4.12 GHz), (d) f_1 = 2.4 GHz, k_1 = 1.4, k_2 = 1.5 (f_2 = 3.36 GHz, f_3 = 5.04 GHz).

The results obtained for both antennas are consistent: modelling the feature-point coordinates instead of the complete responses allows for achieving a considerably better predictive power of the surrogate. At the same time, a very small number of training samples is required to set up an accurate model.

The results of antenna optimization, carried out for the sake of supplemental verification, have been shown in Table 4 and Fig. 7. The process was executed for four selected pairs of the target operating frequencies, using the feature-based nested kriging surrogate set up with 50 training samples. Here, the quality of the initial designs $\boldsymbol{x}^{(0)} = \boldsymbol{s}_I(\boldsymbol{f}_t)$ is not as good as in the case of Antenna I. Nevertheless, the operating frequencies of the optimized designs are allocated as required.

3. Conclusions

The paper proposed a framework for low-cost surrogate modelling of multi-band antennas. Our methodology employs the nested kriging technique and the response feature approach. A combination of domain confinement with restricting the modelling process to the selected characteristic points of the antenna responses permits rendering reliable surrogates using very small training data sets. Our methodology is validated through dual- and triple-band antennas and favourably compared to the benchmark techniques, conventional data-driven models and the nested kriging operating on the entire antenna responses.

The surrogates constructed at the level of selected feature points do not carry full information about the relevant antenna characteristics. On the other hand, focusing the scope of the model on the coordinates of important portions of the responses (here, resonance allocation) leads to a dramatic reduction of the EM simulation data that needs to be acquired to secure the appropriate predictive power of the surrogate. The adequacy of such a model depends on its intended use. Having in mind that parametric optimization is one of the most commonly executed tasks, the provided application examples do demonstrate that the presented framework might be a useful antenna design tool.

Acknowledgement

The authors would like to thank Dassault Systemes, France, for making CST Microwave Studio available. This work is partially supported by the Icelandic Centre for Research RANNIS) Grant 174114051 and by National Science Centre of Poland Grant 2018/31/B/ST7/02369.

References

[1] Khai Nguyen, T.Q., Lizzi, L., Ferrero F.: 'Dual-matching for single resonance miniaturized antenna for IoT applications'. *IEEE Int. Symp. Ant. Prop. (APS/URSI)*, Boston, MA, July 2018, pp. 793–794

[2] Hong, W., Lim, S., Ko, S., Kim, Y.G.: 'Optically invisible antenna integrated within an OLED touch display panel for IoT applications', *IEEE Trans. Ant. Prop.*, 2017, **65**, (7), pp. 3750–3755

[3] Varkiani, S.M.H., Afsahi, M.: 'Compact and ultra-wideband CPW-fed square slot antenna for wearable applications,' *AEU – Int. J. Electr. Comm*, 2019, **106**, pp. 108-115

[4] Wong, H., Lin, W., Huitema, L., Arnaud, E.: 'Multi-polarization reconfigurable antenna for wireless biomedical system', *IEEE Trans. Biomed. Circuits Syst.*, 2017, **11**, (3), pp. 652–660

[5] Siddiqui, J.Y., Saha, C., Antar, Y.M.M.: 'A novel ultrawideband (UWB) printed antenna with a dual complementary characteristic', *IEEE Ant. Wireless Propag. Lett.*, 2015, **14**, pp. 974–977

[6] Goswami, C., Ghatak, R., Poddar, D.R.: 'Multi-band bisected Hilbert monopole antenna loaded with multiple subwavelength split-ring resonators', *IET Microw. Ant. Prop.*, 2018, **12**, (10), pp. 1719–1727

[7] Singh, J., Stephan, R., Hein, M.A.: 'Low-profile penta-band automotive patch antenna using horizontal stacking and corner feeding', *IEEE Access*, 2019, **7**, pp. 74198–74205

[8] Altaf, A., Seo, M.: 'A tilted-D-shaped monopole antenna with wide dual-band dual-sense circular polarization', *IEEE Ant. Wireless Propag. Lett.*, 2018, **17**, (12), pp. 2464–2468

[9] Kumar, P., Dwari, S., Saini, R.K., Mandal, M.K.: 'Dual-band dual-sense polarization reconfigurable circularly polarized antenna', *IEEE Ant. Wireless Propag. Lett.*, 2019, **18**, (1), pp. 64–68

[10] Prabhu, P., Malarvizhi, S.: 'Novel double-side EBG based mutual coupling reduction for compact quad port UWB MIMO antenna,' *AEU – Int. J. Electr. Comm*., 2019, **109**, 146–156

[11] Nie, L.Y., Lin, X.Q., Yang, Z.Q., Zhang, J., Wang, B.: 'Structure-shared planar UWB MIMO antenna with high isolation for mobile platform', *IEEE Trans. Ant. Prop.*, 2019, **67**, (4), pp. 2735–2738

[12] Wolosinski, G., Fusco, V., Naeem, U., Rulikowski, P.: 'Pre-matched eigenmode antenna with polarization and pattern diversity', *IEEE Trans. Ant. Prop.*, 2019, **67**, (8), pp. 5145–5153
[13] Kumar, G., Kumar, R.: 'A survey on planar ultra-wideband antennas with band notch characteristics: Principle, design, and applications,' *AEU – Int. J. Electr. Comm.*, 2019, **109**, pp. 76–98
[14] Koziel, S, Kurgan, P.: 'Selection of circuit geometry for miniaturized microwave components based on concurrent optimization of performance and layout area', *AEU – Int. J. Electr. Comm*., 2019, **109**, pp. 287–294
[15] Ren, Z., Zhao, A., Wu, S.: 'MIMO Antenna with compact decoupled antenna pairs for 5G mobile terminals', *IEEE Ant. Wireless Propag. Lett.*, 2019, **18**, (7), pp. 1367–1371
[16] Koziel, S., Pietrenko-Dabrowska, A.: 'Reduced-cost EM-driven optimization of antenna structures by means of trust-region gradient-search with sparse Jacobian updates', *IET Microw. Ant. Prop.*, 2019, **13**, (10), pp. 1646–1652
[17] Bautista, A., Franc, A., Ferrari, P.: 'Accurate parametric electrical model for slow-wave CPW and application to circuits design', *IEEE Trans. Microwave Theory Techn.*, 2015, **63**, (12), pp. 4225–423
[18] Ciccazzo, A., Di Pillo, G., Latorre, V.: 'A SVM surrogate model-based method for parametric yield optimization', *IEEE Trans. CAD Int. Circ. Syst.*, 2016, **35**, (7), pp. 1224–1228
[19] Koziel, S., Bekasiewicz, A., Cheng, Q.S.: 'Response features for low-cost statistical analysis and tolerance-aware design of antennas', *Int. J. Numer. Model.*, 2018, **31**, (3), e2297
[20] Abd El-Hameed, A.S., Wahab, M.G., Elboushi, A., Elpeltagy, M.S.: 'Miniaturized triple band-notched quasi self-complementary fractal antenna with improved characteristics for UWB applications', *AEU – Int. J. Electr. Comm.*, 2019, **108**, pp. 163–171
[21] Koziel, S., Ogurtsov, S.: '*Simulation-based optimization of antenna arrays*' (World Scientific, Singapur, 2019)
[22] Sobester, A., Forrester, A.I.J., Toal, D.J.J., Tresidder, E., Tucker, S.: 'Engineering design applications of surrogate-assisted optimization techniques', *Optim. Eng.*, 2012, **15**, (1), pp. 243–265
[23] Baratta, I.A., de Andrade, C.B., de Assis, R.R., Silva, E.J.: 'Infinitesimal dipole model using space mapping optimization for antenna placement', *IEEE Ant. Wireless Propag. Lett.*, 2018, **17**, (1), pp. 17–20
[24] Xu, J., Li, M., Chen, R. 'Space mapping optimisation of 2D array elements arrangement to reduce the radar cross-scattering', *IET Microw. Ant. Prop.*, 2017, **11**, (11), pp. 1578–1582
[25] Koziel, S., Leifsson, L.: '*Simulation-driven design by knowledge-based response correction techniques*' (Springer, New York, 2016)
[26] Koziel, S., Bekasiewicz, A.: 'Expedited simulation-driven design optimization of UWB antennas by means of response features', *Int. J. RF Microw. CAE*, 2017, **27**, (6), pp. 1–8

[27] Koziel, S., Unnsteinsson, S.D.: 'Expedited design closure of antennas by means of trust-region-based adaptive response scaling', *IEEE Ant. Wireless Propag. Lett.*, 2018, **17**, (6), pp. 1099–1103
[28] Koziel, S., Bekasiewicz, A.: '*Multi-objective design of antennas using surrogate models*' (World Scientific, Singapur, 2016)
[29] Lophaven, S.N., Nielsen, H.B., Søndergaard, J.: '*DACE: a Matlab kriging toolbox*', Tech. University of Denmark, 2002
[30] Gorissen, D., Crombecq, K., Couckuyt, I., Dhaene, T., Demeester, P.: 'A surrogate modeling and adaptive sampling toolbox for computer based design', *J. Machine Learn. Res.*, 2010, **11**, pp. 2051–2055
[31] Marelli, S., Sudret, B.: 'Uqlab: A framework for uncertainty quantification in Matlab', Int. Conf. Vulner. Risk Analysis Manag. (ICVRAM), Liverpool, United Kingdom, July 2014, pp. 2554–2563
[32] Hassan, A.S.O., Etman, A.S., Soliman, E.A.: 'Optimization of a novel nano antenna with two radiation modes using kriging surrogate models', *IEEE Photon. Journal*, 2018., **10**, (4), pp. 1–17
[33] Dong, J., Li, Q., Deng,L.: 'Fast multi-objective optimization of multi-parameter antenna structures based on improved MOEA/D with surrogate-assisted model', *AEU – Int. J. Electr. Comm.*, 2017, **72**, pp. 192–199
[34] Mishra, S., Yadav, R.N., Singh, R.P.: 'Directivity estimations for short dipole anten-na arrays using radial basis function neural networks', *IEEE Ant. Wireless Propag. Lett.*, 2015, **14**, pp. 1219–1222
[35] Jacobs, J.P.: 'Efficient resonant frequency modeling for dual-band microstrip antennas by gaussian process regression', *IEEE Ant. Wireless Propag. Lett.*, 2015, **14**, pp. 337–341
[36] Chávez-Hurtado, J.L., Rayas-Sánchez, J.E.: 'Polynomial-based surrogate modeling of RF and microwave circuits in frequency domain exploiting the multinomial theorem', *IEEE Trans. Microwave Theory Tech.*, 2016, **64**, (12), pp. 4371–4381
[37] Rayas-Sánchez, J.E.: 'EM-based optimization of microwave circuits using artificial neural networks: the state-of-the-art', *IEEE Trans. Microwave Theory Techn.*, 2004, **52**, (1), pp. 420–435
[38] Prado, D.R., López-Fernández, J.A., Arrebola, M., Goussetis, G.: 'Support vector regression to accelerate design and crosspolar optimization of shaped-beam reflectarray antennas for space applications', *IEEE Trans. Ant. Prop.*, 2019, **67**, (3), pp. 1659–1668
[39] Jacobs, J.P.: 'Bayesian support vector regression with automatic relevance determination kernel for modeling of antenna input characteristics', *IEEE Trans. Antennas Propag.*,2012, **60**, (4), pp. 2114–2118
[40] Easum, J.A., Nagar, J., Werner, D.H.: 'Multi-objective surrogate-assisted optimization applied to patch antenna design', IEEE Int. Symp. Ant. Prop. (APS/URSI), San Diego, CA, July 2017, pp. 339–340
[41] Gehani, A., Agnihotri, P., Pujara, D.A.: 'Analysis and synthesis of multiband Sierpinski carpet fractal antenna using hybrid neuro-fuzzy model', *Progr. In Electromag. Research Lett.*, 2017, **68**, pp. 59–65
[42] Wu, X., Peng, X., Chen, W., Zhang, W.: 'A developed surrogate-based optimization framework combining HDMR-based modeling technique and TLBO

algorithm for high-dimensional engineering problems', *Struct. Multidisc. Optim.*, 2019, **60**, (2), pp. 663–680
[43] Lambert, R.S.C., Lemke, F., Kucherenko, S.S., Song, S., Shah, N.: 'Global sensitivity analysis using sparse high dimensional model representations generated by the group method of data handling', *Math. Comp. Simul.*, 2016, **128**, pp. 42–54
[44] Koziel, S., Bekasiewicz, A.: 'Computationally feasible narrow-band antenna modeling using response features', *Int. J. RF Microwave CAE*, 2017, **27**, (4), e21077
[45] Wen, J., Zhou, Z., Wang, J., Tang, X., Mo, Q.: 'A sharp condition for exact support recovery with orthogonal matching pursuit', *IEEE Trans. Signal Proc.*, 2017, **65**, (6), pp. 1370–1382
[46] Tu, S., Cheng, Q.S., Zhang, Y., Bandler, J.W., Nikolova, N.K.: 'Space mapping optimization of handset antennas exploiting thin-wire models', *IEEE Trans. Ant. Prop.*, 2013, **61**, (7), pp. 3797–3807
[47] Xu, J., Li, M., Chen, R.: 'Space mapping optimisation of 2D array elements arrangement to reduce the radar cross-scattering', *IET Microwaves Ant. Propag.*, 2017, **11**, (11), pp. 1578–1582
[48] Tao, J., Wang, F., Cachecho, P., Zhang, W., Sun, S., Li, X., Kanj, R., Gu, C., Zeng, X.: 'Large-scale circuit performance modeling by bayesian model fusion', in: Elfadel, I., Boning, D., Li, X. (Eds.): '*Machine learning in VLSI Computer-Aided Design*' (Springer, Cham, Germany, 2019)
[49] Koziel, S., Bekasiewicz, A., Couckuyt, I., Dhaene, T.: 'Efficient multi-objective simulation-driven antenna design using co-kriging', *IEEE Trans. Ant. Prop.*, 2014, **62**, (11), pp. 5900–5905
[50] Jacobs, J.P., Koziel, S.: 'Reduced-cost microwave filter modeling using a two-stage Gaussian process regression approach', *Int. J. RF Microwave CAE*, 2015, **25**, 453–462
[51] Koziel S.: 'Low-cost data-driven surrogate modeling of antenna structures by constrained sampling', *IEEE Ant. Wireless Propag. Lett.*, 2017, **16**, pp. 461–464
[52] Koziel S, Sigurðsson AT.: 'Triangulation-based constrained surrogate modeling of antennas', *IEEE Ant. Wireless Propag. Lett.*, 2018, **66**, (8), pp. 4170–4179
[53] Koziel, S., Pietrenko-Dabrowska, A.: 'Performance-based nested surrogate modeling of antenna input characteristics', *IEEE Trans. Ant. Prop.*, 2019, **67**, (5), pp. 2904–2912
[54] Koziel, S., Pietrenko-Dabrowska, A.: 'Computationally-efficient and reliable surrogate modeling of antenna structures using performance-driven nested kriging', 2019 IEEE MTT-S International Conference on Numerical Electromagnetic and Multiphysics Modeling and Optimization (NEMO), Boston, MA, May 2019, pp. 1–4
[55] Koziel, S., Pietrenko-Dabrowska, A.: 'Reliable data-driven modeling of high-frequency structures by means of nested kriging with enhanced design of experiments', *Eng. Comp.*, 2019, **36**, (7), pp. 2293-2308
[56] Koziel, S., Pietrenko-Dabrowska, A.: 'Surrogate modeling of high-frequency structures using nested kriging and improved sampling strategy', International Conference on Electromagnetics in Advanced Applications (ICEAA), Granada, Spain, 2019, pp. 0066-0069

[57] Simpson, T.W., Peplinski, J.D., Koch, P.N., Allen, J.K.: 'Metamodels for computer-based engineering design: Survey and recommendations', *Eng. Computers*, 2001, **17**, pp. 129-150
[58] Koziel, S.: 'Fast simulation-driven antenna design using response-feature surrogates', *Int. J. RF & Microwave CAE*, 2015, **25**, (5), pp. 394–402
[59] Beachkofski, B., Grandhi, R.: 'Improved distributed hypercube sampling', American Institute of Aeronautics and Astronautics, *Paper AIAA*, 2002, 2002-1274
[60] Chen, Y.-C., Chen, S.-Y., Hsu P.: 'Dual-band slot dipole antenna fed by a coplanar waveguide', IEEE Ant. Propag. Society Int. Symp., Albuquerque, NM, July 2006, pp. 3589–3592
[61] Koziel, S., Bekasiewicz, A.: 'Fast re-design and geometry scaling of multi-band antennas using inverse surrogate modeling techniques', *Int. J. Num. Model.*, 2018, **31**, (3), pp. 1–11